

13. Stuiver, M. & Reimer, P. J. Extended ^{14}C data base and revised CALIB 3.0 ^{14}C age calibration program. *Radiocarbon* **35**, 215–230 (1993).

14. Grove, J. M. *The Little Ice Age* (Methuen, London, 1988).

15. Mayewski, P. A. *et al.* Changes in atmospheric circulation and ocean ice cover over the North Atlantic during the last 41,000 years. *Science* **263**, 1747–1751 (1994).

16. Brown, P., Kennett, J. P. & Ingram, B. L. Marine evidence for episodic Holocene megafloods in North America and the northern Gulf of Mexico. *Paleoceanography* **14**, 498–510 (1999).

17. Knox, J. C. Sensitivity of modern and Holocene floods to climate change. *Quat. Sci. Rev.* **19**, 439–457 (1999).

18. Lamb, H. H. Variation and changes in the wind and ocean circulation: the Little Ice Age in the northeast Atlantic. *Quat. Res.* **11**, 1–20 (1979).

19. Liu, K. B. & Fearn, M. L. Reconstruction of prehistoric landfall frequencies of catastrophic hurricanes in northwestern Florida from lake sediment records. *Quat. Res.* **54**, 238–245 (2000).

20. Zong, Y. & Tooley, M. J. Evidence of mid-Holocene storm-surge deposits from Morecambe Bay, northwest England: A biostratigraphical approach. *Quat. Int.* **55**, 43–50 (1999).

21. O'Brien, S. R. *et al.* Complexity of Holocene climate as reconstructed from a Greenland ice core. *Science* **270**, 1962–1964 (1995).

22. Fischer, H. Imprint of large-scale atmospheric transport patterns on sea-ice records in northern Greenland ice cores. *J. Geophys. Res.* **106**, 23977–23984 (2001).

23. Hormes, A., Müller, B. U. & Schlüchter, C. The Alps with little ice: evidence for eight Holocene phases of reduced glacier extent in the Central Swiss Alps. *Holocene* **11**, 255–265 (2001).

24. Karlén, W. & Kuylenstierna, J. On solar forcing of Holocene climate: evidence from Scandinavia. *Holocene* **6**, 359–365 (1996).

25. Boulton, G. S., *et al.* *Glacier Fluctuations during the Holocene* (eds Frenzel, B., Boulton, G. S., Gläser, B. & Huckriede, U.) 5–23 (Fischer, Stuttgart, 1997).

26. Matthews, J. A., Dahl, S. O., Nesje, A., Berrisford, M. & Andersson, C. Holocene glacier variations in central Jotunheimen, southern Norway based on distal glaciolacustrine sediment cores. *Quat. Sci. Rev.* **19**, 1625–1647 (2000).

27. Bond, G. *et al.* Persistent solar influence on North Atlantic climate during the Holocene. *Science* **294**, 2130–2136 (2001).

28. Shindell, D. T., Schmidt, G. A., Mann, M. E., Rind, D. & Waple, A. Solar forcing of regional climate change during the Maunder minimum. *Science* **294**, 2149–2152 (2001).

29. Thomson, D. J. Spectrum estimation and harmonic analysis. *Proc. IEEE* **70**, 1055–1096 (1982).

30. Mann, M. E. & Lees, J. M. Robust estimation of background noise and signal detection in climatic time series. *Clim. Change* **33**, 409–445 (1996).

Supplementary Information accompanies the paper on Nature's website (<http://www.nature.com/nature>).

Acknowledgements We thank J. Galster for field and laboratory assistance, K. Jennings for field assistance, A. Bosley and A. Conlan for grain size analysis, S. Brown for laboratory training, P.T. Davis for coring device design and training, and J. M. Wallace and H. Fischer for comments and discussion. This work was supported by the US National Science Foundation (P.R.B.).

Competing interests statement The authors declare that they have no competing financial interests.

Correspondence and requests for materials should be addressed to A.J.N. (e-mail: anders.noren@alumni.carleton.edu).

The strength of $\text{Mg}_{0.9}\text{Fe}_{0.1}\text{SiO}_3$ perovskite at high pressure and temperature

Jiuhua Chen, Donald J. Weidner & Michael T. Vaughan

Mineral Physics Institute and Department of Geosciences, State University of New York at Stony Brook, Stony Brook, New York 11794–2100, USA

The Earth's lower mantle consists mainly of $(\text{Mg,Fe})\text{SiO}_3$ perovskite and $(\text{Mg,Fe})\text{O}$ magnesiowüstite, with the perovskite taking up at least 70 per cent of the total volume¹. Although the rheology of olivine, the dominant upper-mantle mineral, has been extensively studied, knowledge about the rheological behaviour of perovskite is limited. Seismological studies indicate that slabs of subducting oceanic lithosphere are often deflected horizontally at the perovskite-forming depth, and changes in the Earth's shape and gravity field during glacial rebound indicate that viscosity increases in the lower part of the mantle. The rheological properties of the perovskite may be important in governing these phenomena. But $(\text{Mg,Fe})\text{SiO}_3$ perovskite is not

stable at high temperatures under ambient pressure, and therefore mechanical tests on $(\text{Mg,Fe})\text{SiO}_3$ perovskite are difficult. Most rheological studies of perovskite have been performed on analogous materials^{2–7}, and the experimental data on $(\text{Mg,Fe})\text{SiO}_3$ perovskite are limited to strength measurements at room temperature in a diamond-anvil cell⁸ and microhardness tests at ambient conditions⁹. Here we report results of strength and stress relaxation measurements of $(\text{Mg}_{0.9}\text{Fe}_{0.1})\text{SiO}_3$ perovskite at high pressure and temperature. Compared with the transition-zone mineral ringwoodite¹⁰ at the same pressure and temperature, we found that perovskite is weaker at room temperature, which is consistent with a previous diamond-anvil-cell experiment⁸, but that perovskite is stronger than ringwoodite at high temperature.

The perovskite sample was synthesized at 26 GPa and 2,100 K from a glass of composition $(\text{Mg}_{0.9}\text{Fe}_{0.1})\text{SiO}_3$. X-ray diffraction confirmed the pure perovskite phase. *In situ* stress measurements were performed using a large-volume press (SAM85) at the X17B beamline of the National Synchrotron Light Source¹¹. Stress in the sample was measured by monitoring the broadening of diffraction peaks from the sample at high pressure and temperature. The experiment is described briefly below; details of the methodology, along with previous studies on mantle-related materials, can be found elsewhere^{10,12,13}.

The synthesized sample was powdered at liquid-nitrogen temperature to prevent amorphization, and loaded into a high-pressure cell together with a layer of NaCl as an internal pressure calibrant. The experiment was conducted by first increasing the pressure to 20 GPa, and then increasing the temperature. At each temperature, energy-dispersive X-ray diffraction patterns were collected as a function of time to characterize the stress relaxation. The sample pressure was monitored by comparing the compression of NaCl to the Decker scale¹⁴, and the sample temperature was measured by a W_{97}Re_3 – $\text{W}_{75}\text{Re}_{25}$ thermocouple. In all the X-ray diffraction patterns from the sample at the pressures and temperatures reported here, no back transformation was observed. When temperature was later increased above 1,273 K, the diffraction pattern showed a back transformation in the sample because the experiment was carried out at a pressure lower than the perovskite stability field. Our stress measurements are therefore limited to the data collected up to 1,073 K.

Heterogeneous deviatoric stress at each grain of the powdered sample, together with very small grain sizes, gives rise to diffraction

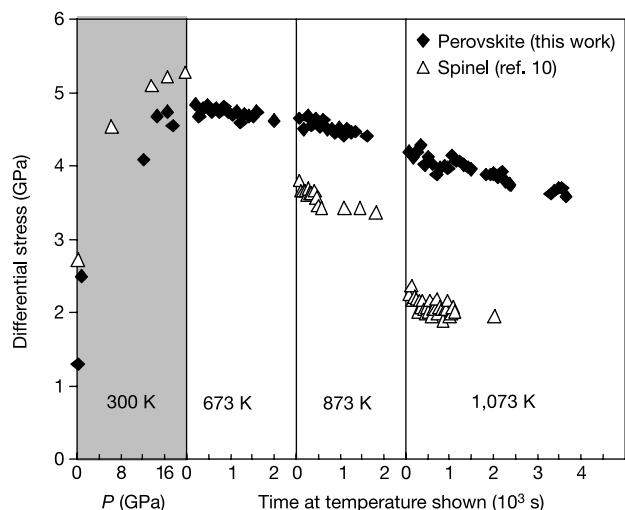


Figure 1 Differential stress supported by $\text{Mg}_{0.9}\text{Fe}_{0.1}\text{SiO}_3$ perovskite and Mg_2SiO_4 spinel as a function of time at several constant temperatures under ~ 20 -GPa confining pressure. Filled diamonds, perovskite (this work); open triangles, spinel (from previous study¹⁰). Data in the shaded area correspond to stresses of the sample during loading.

peak broadening. In the case of energy dispersive X-ray diffraction, stress-induced peak broadening is proportional to the photon energy of the X-ray, whereas the broadening caused by small grain size is energy independent¹⁵, that is:

$$\text{FWHM}^2 = (2\varepsilon E)^2 + (Kh c/2P \sin \Theta_0)^2$$

where FWHM represents the sample contribution to the peak broadening (full-width at half-maximum of a gaussian profile), 2ε is the differential strain (which is equal to the differential stress multiplied by the aggregate Young's modulus (442.4 GPa is used for the perovskite)), E is the X-ray photon energy, K is the Scherrer constant, h is Planck's constant, c is the velocity of light, P is the average grain size, and $2\theta_0$ is the fixed scattering angle. The results reported here are derived by deconvoluting the peak broadening of the sample diffraction patterns from observed signal^{10,13}.

Figure 1 shows the measured differential stress supported by the perovskite sample as a function of time. The grey panel shows data obtained as pressure was first increased at 300 K; the other panels show data obtained at several other constant temperatures at ~20-GPa confining pressure. For comparison, the data for γ -Mg₂SiO₄ spinel (ringwoodite)¹⁰ are superposed on the plot. The stresses in both the perovskite and the ringwoodite samples increase with load pressure, and a downward curvature of the stress versus load pressure indicates plastic yielding of the sample. At room temperature, the strength of the (Mg_{0.9}Fe_{0.1})SiO₃ perovskite is about 0.5 GPa lower than that of the ringwoodite. However, the perovskite becomes much stronger relative to the ringwoodite at higher temperatures. At 873 K, the strength of the (Mg_{0.9}Fe_{0.1})SiO₃ perovskite is about 1 GPa higher than that of the ringwoodite, and the difference increases to 2 GPa at 1,073 K. We find that the strength of perovskite at room temperature is slightly less than that of ringwoodite; this result is qualitatively consistent with that of ref. 8. However, at high temperature, the perovskite is definitely stronger than the ringwoodite.

All of these measurements are in a regime of high stress and relatively low temperature. At these conditions, there are a few possible deformation mechanisms that may be operative. Assuming a constant total strain (elastic + plastic) during the relaxation process¹³, we derived the plastic strain rate from the time-resolved data at temperatures of 673 K, 873 K and 1,073 K in order to explore the possible operative mechanism. Dislocation glide is often the dominant deformation mechanism under high stress and low

temperature¹⁶. The strain rate is generally described by the Arrhenius equation:

$$\dot{\varepsilon} = A_1 \left(\frac{\sigma}{\mu} \right)^2 \exp(-Q(\sigma)/RT) \quad (1)$$

where $\dot{\varepsilon}$ is the strain rate, A_1 a constant, μ the shear modulus, R the gas constant, T the temperature, and Q the activation energy (which is a function of the stress σ). We could not find an adequate set of parameters to fit the experimental data at all three temperatures. When we divided the data into two sets—(1) 673 K and 873 K, and (2) 873 K and 1,073 K—and expressed the stress effect on Q as $Q(1 - \sigma/\tau)$, where τ represents the Peierls stress (that is, lattice friction stress at temperature of 0 K), we found that both τ and Q change as a function of temperature (5.8 GPa and 183 kJ mol⁻¹ for case (1); 7.6 GPa and 236 kJ mol⁻¹ for case (2)).

Another possible deformation mechanism is power-law creep by climb-plus-glide, which is characterized by:

$$\dot{\varepsilon} = A_2 \frac{D_v}{RT} \left(\frac{\sigma}{\mu} \right)^n \quad (2)$$

where A_2 is a constant, and D_v the lattice diffusion coefficient. The exponent n normally varies from 3 to 10. However, the stress relaxation in the perovskite is so slow that the derived exponent n is about one order of magnitude higher than the typical values. Therefore this power-law creep is also unlikely to be the operative mechanism.

Thus it is likely that among the competing deformation mechanisms in the perovskite system, some other relaxation process is weaker than dislocation glide and power-law creep, and hence controls the strength in this temperature region. One possibility is twinning. Twinning domains are easily generated in (Mg,Fe)SiO₃ perovskite on (110) and (112) planes because of its ferroelastic character¹⁷. The (110) twinning results in an interchange of the a and b axes between adjacent twin domains^{18,19}, and can be induced by differential stress. Under a cylindrical stress field, as in our experiment¹¹, the twinning on the (110) plane during compression gives rise to an increase of relative diffraction intensity ($I_{(200)}/I_{(020)}$) in the perovskite structure²⁰. Because of the clear observation of such features in our experiment (Fig. 2) and the support from the previous related studies²⁰, we suggest that mechanical twinning may be a favourable candidate for an operative deformation mechanism in the (Mg,Fe)SiO₃ perovskite under the high-stress and low-temperature regime. However, this suggestion still needs to be confirmed by some more-direct evidence, although the preferred mechanical twinning mechanism with respect to dislocation glide at low temperature is also observed in other minerals²¹. Although the strain rate for the twinning mechanism can be estimated by an equation similar to equation (1), it has been demonstrated that both effective activation energy (Q) and twinning nucleation stress (τ) are temperature dependent¹⁶. This is consistent with the characteristics of our data.

On the other hand, another mechanism—dynamic recrystallization—is known to produce strength that may have a weak temperature dependence in some cases^{22,23}. This process might also seem to be a potential candidate for the operative deformation mechanism because of the observed weak temperature dependence of the perovskite strength (Fig. 1). But dynamic recrystallization has been documented to take place mostly at high temperature ($T > 0.6T_m$)¹⁶, T_m being the melting temperature and our data are limited to the temperatures $< 0.5T_m$.

Although the operative deformation mechanism is not known for sure, our experiments show that perovskite is very strong (stronger than ringwoodite) at these conditions. If twinning is the mechanism, it could only operate for small strains and would not be viable once the entire sample had obtained the minimum-energy twin state: a stronger deformation mechanism might then become

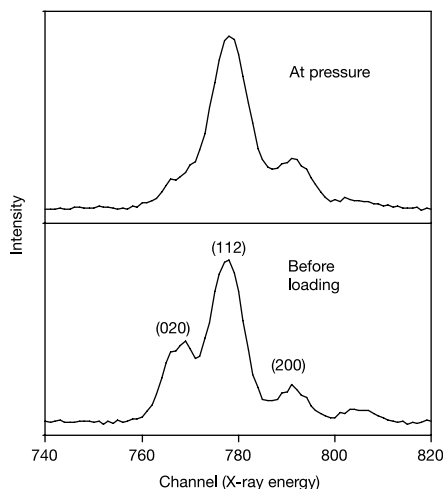


Figure 2 Change in the relative intensities of the (020) and (200) diffraction peaks of Mg_{0.9}Fe_{0.1}SiO₃ perovskite owing to compression. The data from the compressed sample indicate an increase in the population of (200)-oriented grains (parallel to the loading axis) relative to (020)-oriented grains. This is evidence for a twinning process that converts the b axis to the shorter a axis under uniaxial loading (see text).

operative. The current result represents the lower limits of strength of the perovskite at these conditions.

We note that the pressure, temperature and stress levels in our experiment are not the same as the conditions in the Earth's lower mantle, where the temperature is probably 1,000 K higher and the stress level is about two orders of magnitude lower. Therefore the deformation mechanism probably falls into a different regime, and the current result can not be directly applied to the lower mantle. But this study reveals the rheological behaviour of (Mg,Fe)SiO₃ perovskite at high pressure and temperature, and suggests a revision of expectations that are based on room-temperature results⁸. It is probably more reasonable to predict the rheological behaviour of perovskite in the mantle from the present high-pressure and high-temperature experimental result, than from high-pressure but room-temperature data. Under the experimental conditions, using the data for both perovskite and ringwoodite (Fig. 1), we estimated the viscosity ($\eta = \sigma/\dot{\epsilon}$) of perovskite to be one order of magnitude higher than that of ringwoodite at 1,073 K. Once again, as the deformation in the Earth's lower mantle is likely to be dominated by diffusion creep, a more accurate comparison should be made on the basis of the diffusion creep data when they become available.

On the other hand, 1,073 K is a very reasonable temperature to be expected in subducted slabs at the bottom of the transition zone. Our experiment clearly shows that at this temperature perovskite is definitely much stronger than ringwoodite. This fact helps to explain why some subducted slabs deflect at top of the lower mantle, as the perovskite may create a mechanical barrier to subduction of the weaker ringwoodite²⁴. Ultimately, the determination of the relative strengths of the different media must also consider other characteristics, such as grain-size effects as discussed by Karato *et al.*²⁵. These authors showed that coarsening of the grain size increases the slab strength, and therefore a coarse-grained slab can penetrate into the lower mantle.

The mechanism of deep-focus earthquakes along subducted slabs has been a long-standing question, because the traditional brittle failure model is not likely to be operative in the deep mantle. With the progress in understanding the rheological properties of minerals, the early model of a thermal runaway instability^{26,27}—when deformation of a material occurs so rapidly that heat is accumulated in the region of high strain—has regained special attention^{25,28}. Using existing rheology data, Karato *et al.*²⁵ have modelled the rheological structure of subducted slabs in a fashion that satisfies the depth variation of seismicity down to the bottom of the transition zone. Lacking the rheology data for perovskite, these authors inferred that the clear shut-off of seismicity at the top of the lower mantle is probably attributable to loss of strength of the slabs in this depth region, owing to superplasticity and/or the absence of strong forces. In fact, following the thermal runaway instability model, thermal weakening (for example, the temperature-sensitive strength of olivine and ringwoodite¹⁰) enhances the positive feedback between deformation-induced heating and deformation. If the subducted slabs in the lower mantle consist of cold perovskite which does not weaken significantly with temperature as we observed (Fig. 1), the thermal runaway instability may not be promoted, with the result that earthquakes would not occur in the perovskite portion of the slab. □

Received 27 March; accepted 12 September 2002; doi:10.1038/nature01130.

- Anderson, D. L. & Bass, J. D. Transition region of the Earth's upper mantle. *Nature* **320**, 321–328 (1986).
- Poirier, J. P., Peyronneau, J., Gesland, J. Y. & Brebec, G. Viscosity and conductivity of the lower mantle: an experimental study on a MgSiO₃ perovskite analogue, KZnF₃. *Phys. Earth Planet. Inter.* **32**, 273–287 (1983).
- Doukhan, N. & Doukhan, J. C. Dislocation in perovskite BaTiO₃ and CaTiO₃. *Phys. Chem. Miner.* **13**, 403–410 (1986).
- Karato, S.-i. Plasticity-crystal structure systematics in dense oxides and its implications for the creep strength of the Earth's deep interior: a preliminary result. *Phys. Earth Planet. Inter.* **55**, 234–240 (1989).
- Karato, S.-i. & Li, P. Diffusion creep in perovskite: implications for the rheology of the lower mantle. *Science* **255**, 1238–1240 (1992).

- Li, P., Karato, S.-i. & Wang, Z. High-temperature creep in fine-grained polycrystalline CaTiO₃, an analogue material of (Mg,Fe)SiO₃ perovskite. *Phys. Earth Planet. Inter.* **95**, 19–36 (1996).
- Wright, K., Price, G. D. & Poirier, J. P. High-temperature creep of the perovskite CaTiO₃ and NaNbO₃. *Phys. Earth Planet. Inter.* **74**, 9–22 (1992).
- Meade, C. & Jeanloz, R. The strength of mantle silicates at high pressures and room temperature: implications for the viscosity of the mantle. *Nature* **348**, 533–535 (1990).
- Karato, S.-i., Fujino, K. & Ito, E. Plasticity of MgSiO₃ perovskite: the results of microhardness tests on single crystals. *Geophys. Res. Lett.* **17**, 13–16 (1990).
- Chen, J., Inoue, T., Weidner, D., Wu, Y. & Vaughan, M. Strength and water weakening of mantle minerals, olivine, wadsleyite and ringwoodite. *Geophys. Res. Lett.* **25**, 575–578 1103–1104 (1998).
- Weidner, D. J., *et al.* *High-pressure Research: Application to Earth and Planetary Sciences* (eds Syono, Y. & Manghnani, M. H.) 13–17 (Terra Scientific/AGU, Tokyo/Washington DC, 1992).
- Weidner, D. J., Wang, Y. & Vaughan, M. T. Yield strength at high pressure and temperature. *Geophys. Res. Lett.* **21**, 753–756 (1994).
- Weidner, D. J., Wang, Y., Chen, G., Ando, J. & Vaughan, M. T. *Properties of Earth and Planetary Materials at High Pressure and Temperature* (eds Manghnani, M. H. & Yagi, T.) 473–482 (Geophysical Monograph, AGU, Washington DC, 1998).
- Decker, D. L. High-pressure equation of state for NaCl, KCl and CsCl. *J. Appl. Phys.* **42**, 3239–3244 (1971).
- Gerward, L., Morup, S. & Topsoe, H. Particle size and strain broadening in energy-dispersive x-ray powder patterns. *J. Appl. Phys.* **47**, 822–825 (1976).
- Frost, H. J. & Ashby, M. F. *Deformation-Mechanism Maps* (Pergamon, Oxford, 1982).
- Wang, Y., Guyot, F., Yeganeh-Haeri, A. & Liebermann, R. C. Twinning in MgSiO₃ perovskite. *Science* **248**, 468–471 (1990).
- Sapriel, J. Domain-wall orientations in ferroelastics. *Phys. Rev. B* **12**, 5128–5140 (1975).
- Toledano, J. C. & Toledano, P. Order parameter symmetries and free-energy expansions for purely ferroelastic transitions. *Phys. Rev. B* **21**, 1139–1172 (1980).
- Zhao, Y. *et al.* High-pressure crystal chemistry of neighborite, NaMgF₃: An angle-dispersive diffraction study using monochromatic synchrotron x-radiation. *Am. Mineral.* **79**, 615–621 (1994).
- Avé Lallemant, H. G. Experimental deformation of diopside and websterite. *Tectonophysics* **48**, 1–27 (1978).
- Derby, B. *Deformation Processes in Minerals, Ceramics and Rocks* (eds Barber, D. J. and Meredith, P. G.) 354–364 (Unwin Hyman, London, 1990).
- Shimizu, I. Stress and temperature dependence of recrystallized grain size: A subgrain misorientation model. *Geophys. Res. Lett.* **25**, 4237–4240 (1998).
- Gurnis, M. & Hager, B. H. Controls of the structure of subducted slabs. *Nature* **335**, 317–321 (1988).
- Karato, S.-i., Riedel, M. R. & Yuen, D. A. Rheological structure and deformation of subducted slabs in the mantle transition zone; implications for mantle circulation and deep earthquakes. *Physics Earth Planet. Inter.* **127**, 83–108 (2001).
- Griggs, D. T. & Baker, D. W. *Properties of Matter Under Unusual Conditions* (eds Mark, H. & Fernbach, S.) 23–42 (Wiley/Interscience, New York, 1969).
- Ogawa, M. Shear instability in a viscoelastic material as the cause of deep focus earthquakes. *J. Geophys. Res.* **92**, 13801–13810 (1987).
- Weidner, D. J. *et al.* Subduction zone rheology. *Phys. Earth Planet. Inter.* **127**, 67–81 (2001).

Acknowledgements This work was carried out at the X17B beamline of the National Synchrotron Light Source. We thank Z. Zhang, J. B. Hastings and D. P. Siddons for technical support at the beamline, and J. Zhang for help in sample preparation. This work was supported by the US National Science Foundation.

Competing interests statement The authors declare that they have no competing financial interests.

Correspondence and requests for materials should be addressed to J.C. (e-mail: jiuhua.chen@sunysb.edu).

Contemporary fisherian life-history evolution in small salmonid populations

Mikko T. Koskinen*, Thron O. Haugen† & Craig R. Primmer*

* Department of Ecology and Systematics, Division of Population Biology, PO Box 65, Viikinkaari 1, FIN-00014, University of Helsinki, Finland

† Department of Biology, Division of Zoology, PO Box 1050, Blindern, N-0316, Oslo, Norway

The relative importance of natural selection¹ and random drift² in phenotypic evolution has been discussed since the introduction of the first population genetic models^{3–5}. The empirical evidence used to evaluate the evolutionary theories of Fisher¹ and Wright² remains obscure because formal tests for neutral divergence^{6–8} or sensitive attempts to separate the effects of